ARTICLES
PUBLISHED ONLINE: 26 JANUARY 2014 | DOI: 10.1038/NGEO2066
nature geoscience

# Tropospheric ozone trends at Mauna Loa Observatory tied to decadal climate variability

Meiyun Lin[1,2]*, Larry W. Horowitz[2], Samuel J. Oltmans[3,4], Arlene M. Fiore[5] and Songmiao Fan[2]

**A potent greenhouse gas and biological irritant, tropospheric ozone is also the primary source of atmospheric hydroxyl radicals, which remove numerous hazardous trace gases from the atmosphere. Tropospheric ozone levels have increased in spring at remote sites in the mid-latitudes of the Northern Hemisphere over the past few decades; this increase has been attributed to a growth in Asian precursor emissions. In contrast, 40 years of continuous measurements at Mauna Loa Observatory in Hawaii reveal little change in tropospheric ozone levels during spring (March–April), but a rise in autumn (September–October). Here we examine the contribution of decadal shifts in atmospheric circulation patterns to variability in tropospheric ozone levels at Mauna Loa using a suite of chemistry–climate model simulations. We show that the flow of ozone-rich air from Eurasia towards Hawaii during spring weakened in the 2000s as a result of La-Niña-like decadal cooling in the eastern equatorial Pacific Ocean. During autumn, in contrast, the flow of ozone-rich air from Eurasia to Hawaii strengthened in the mid-1990s onwards, coincident with the positive phase of the Pacific–North American pattern. We suggest that these shifts in atmospheric circulation patterns can reconcile observed trends in tropospheric ozone levels at Mauna Loa and the northern mid-latitudes in recent decades. We conclude that decadal variability in atmospheric circulation patterns needs to be considered when attributing observed changes in tropospheric ozone levels to human-induced trends in precursor emissions.**

The lifetime of ozone in the free troposphere is sufficiently long (~22 days; ref. 1) that ozone levels at a remote location are influenced by hemispheric precursor emissions[2,3] and large-scale circulation patterns[4–6]. The response of tropospheric ozone to changing atmospheric circulation is poorly understood owing to a lack of reliable long-term observations, but may influence climate, health, agriculture, and atmospheric composition[7]. Continuous ozone measurements have been made at Mauna Loa Observatory (MLO) on the Island of Hawaii (19.5° N, 155.6° W, 3.4 km altitude) since 1973 (refs 8,9). This 40-year time series is unique not only because of its length but also because MLO is near the boundary between the mid-latitude and tropical circulation cells, rendering it sensitive to both intra- and inter-hemispheric mixing. The MLO ozone record provides an unprecedented opportunity to deconstruct the observed ozone changes into components driven by trends in hemispheric precursor emissions versus shifts in circulation regimes.

Efforts to improve air quality have led to decreases in ozone precursor emissions from North America and Europe in the past 20 years, whereas emissions increased markedly in Asia[10–13]. Rising Asian emissions have been implicated in raising baseline ozone mixing ratios observed at northern mid-latitude remote sites[2,9,14–16], with the most pronounced increases in spring when hemispheric pollution transport is greatest[3]. In striking contrast, ref. 17 found that ozone measured at MLO shows no trend in spring from 1973 to 2004, but instead increases in autumn when ozone is at its seasonal minimum. An extended ozone record to 2012 shows a continuation of this trend, with the largest increases occurring in September and October (Fig. 1a). These seasonal ozone trends are corroborated in the independent ozonesonde record at Hilo, Hawaii (Supplementary Fig. 1). The mechanisms controlling these changes in seasonal ozone over the subtropical North Pacific region have not previously been characterized unambiguously, but trends in precursor emissions alone are insufficient to explain the observed changes.

Here we present evidence that the seasonal ozone trends measured at MLO reflect decadal shifts in the circulation regimes, in which airflow from Eurasia towards Hawaii weakened in spring but strengthened in autumn over recent decades. Specifically, we conduct a suite of hindcast simulations with the Geophysical Fluid Dynamic Laboratory global chemistry–climate model (GFDL AM3)[18–20] designed to isolate the response of ozone to historical changes in human-induced emissions of non-methane ozone precursors, methane, wildfires and meteorology (Methods). Our BASE simulation and two additional simulations with modified emissions (FIXEMIS and IAVFIRE) are nudged to reanalysis winds over 1980–2012. We also conduct ensemble simulations without nudging, driven by prescribed sea surface temperatures (SSTs) and atmospheric radiative forcing agents over 1960–2012 (hereafter referred to as the AMIP simulations). These AMIP simulations enable us to determine whether the changes in atmospheric circulation are forced by changes in the tropical ocean.

## Mean transport regimes in spring versus autumn

In boreal spring, airflow from Eurasia dominates transport to MLO owing to a deep Aleutian Low and strong mid-latitude westerly flow (Fig. 2a and Supplementary Fig. 2). MLO is located near the northern edge of the Hadley cell during spring, and thus is sensitive to variability in the subtropical jet location. The El Niño/Southern Oscillation (ENSO), with timescales of two to about seven years, is known to modulate the location and strength of the subtropical

[1]Atmospheric and Oceanic Sciences, Princeton University, Princeton, New Jersey 08540, USA, [2]NOAA Geophysical Fluid Dynamics Laboratory, Princeton, New Jersey 08540, USA, [3]Cooperative Institute for Research in Environmental Sciences, University of Colorado, Boulder, Colorado 80309, USA, [4]NOAA Earth System Research Laboratory, Boulder, Colorado 80305, USA, [5]Department of Earth and Environmental Sciences and Lamont-Doherty Earth-Observatory, Columbia University, Palisades, New York 10964, USA. *e-mail: Meiyun.Lin@noaa.gov

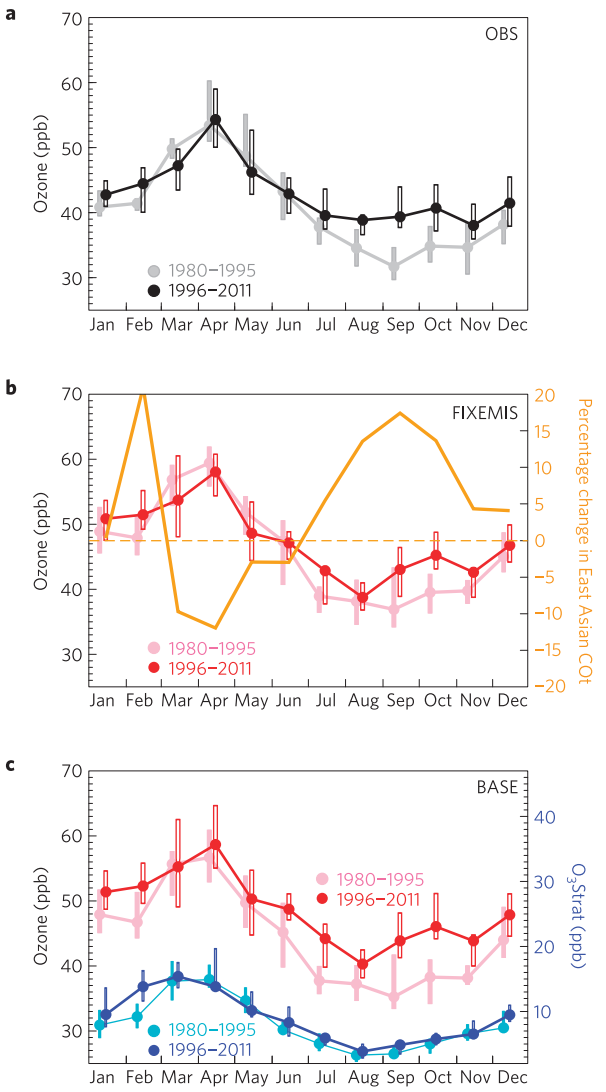


**Figure 1 | The changing ozone seasonal cycle at MLO from 1980–1995 to 1996–2011. a**, Observations. **b**,**c**, GFDL AM3 model simulations with constant (FIXEMIS) and time-varying (BASE) precursor emissions. Symbols represent median values; the vertical bars give the 25–75th percentile range. The orange line in **b**, using the orange axis, indicates percentage changes in East Asian COt (carbon-monoxide-like tracer; see Methods) between two 16-year means (1996–2011 minus 1980–1995). The cyan and blue lines in **c**, using the blue axis, denote estimated ozone of stratospheric origin ($O_3$Strat; see Methods).

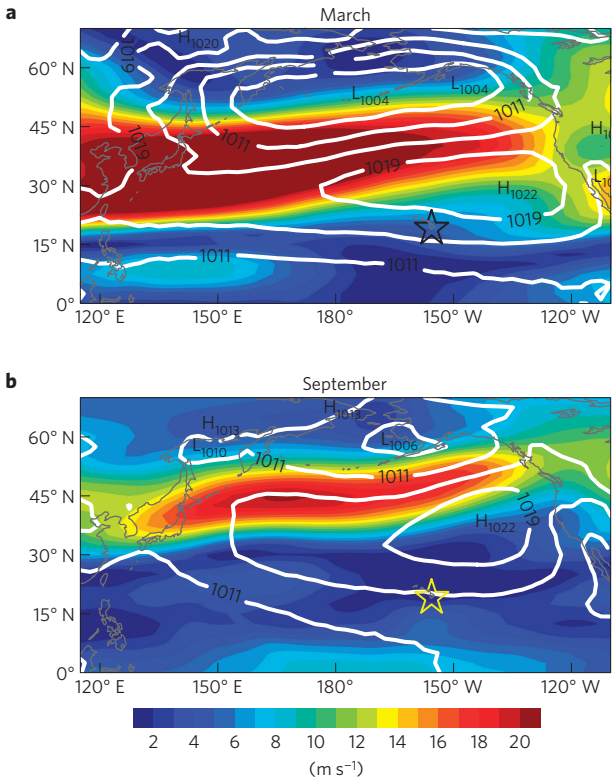


**Figure 2 | Mean climate in spring versus autumn. a**,**b**, March (**a**) and September (**b**) mean sea level pressure (in hPa, contours) superimposed on 500 hPa wind speed (in m s$^{-1}$, shading), based on NCEP/NCAR reanalysis averaged over 1980–2012. The star symbol denotes the location of MLO.

jet in winter and spring[21]. ENSO has exhibited considerable inter-decadal variability over the past century, in association with the Pacific Decadal Oscillation[22,23] (PDO). The position of the subtropical jet varies with the location of the subsiding branch of the Hadley cell, which some observational diagnostics indicate has been expanding since the 1960s (refs 24–27).

In boreal autumn, the subtropical jet is positioned further northward and MLO is located deep in the tropical belt, with a seasonal minimum in airflow from East Asia (Fig. 2b). Therefore, variability in mid-latitude westerlies, influenced by a change in the PDO or in the Hadley circulation, has little impact on MLO ozone levels in autumn. Influence of mid-latitude air at MLO in autumn occurs primarily through long-distance, isentropic subsidence driven by pressure dipoles over the eastern North Pacific. Enhanced ridges near Hawaii, accompanied by a deepening of the Aleutian Low in the North Pacific and development of deep troughs over the southeastern United States, are characteristic of a positive-mode Pacific–North American (PNA) pattern[28,29]. The PNA pattern exhibits variability over a range of timescales from weeks to decades. Although it is influenced by tropical heating on low frequencies, the PNA can also arise internally through atmospheric dynamics in any season except summer[28]. We suggest that the strengthened Pacific subtropical high related to the positive PNA results in anomalous southward transport of ozone-rich mid-latitude air towards Hawaii during autumn when westerly flow is relatively weak.

## Role of emissions versus meteorology

The GFDL AM3 model nudged to reanalysis winds reproduces the seasonal cycle of ozone measured at MLO and captures the distinct seasonal trends (Fig. 1b,c), lending confidence in the utility of the model for attributing observed ozone changes to specific processes. A regional carbon-monoxide-like tracer (East Asian COt; see Methods) in AM3 indicates that the mean influence of Eurasian airflow at MLO decreases by as much as 15% in March and April, but increases by 18% in September and October from 1980–1995 to 1996–2011 (Fig. 1b). The South Asian COt exhibits a similar behaviour to the East Asian COt in spring and the North American COt shows no significant change in any season at MLO (Supplementary Fig. 2).

Ozone in the subtropical free troposphere is also influenced by transport from the stratosphere in winter and spring[4,5,20]. Kona storms, a type of winter extratropical cyclone occurring in the Hawaiian Islands, occasionally transport mid-latitude stratospheric ozone into the lower troposphere at MLO (ref. 30). A stratospheric ozone tracer in AM3 (Methods) demonstrates no significant change in stratospheric ozone transport to MLO except for an increase in February (Fig. 1c).

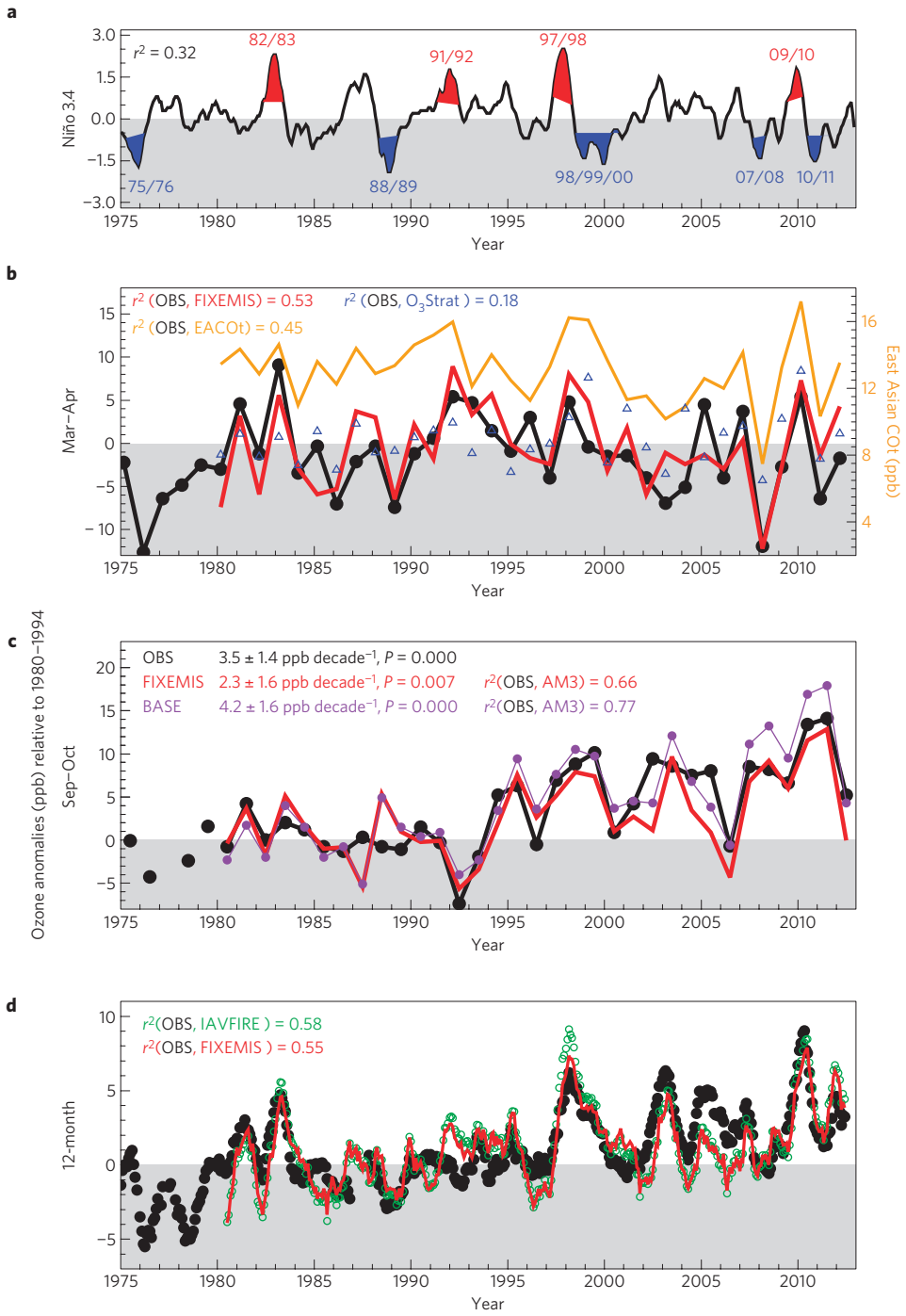


**Figure 3 | Interannual ozone variability at MLO. a**, The Niño 3.4 index, highlighting strong El Niño (red) and La Niña (blue) events (Methods). **b**–**d**, Ozone anomalies relative to 1980–1994 for March–April, September–October, and 12-month running average as observed (black) and simulated with fixed emissions (red), with only fire emissions varying (green), and with both fire and anthropogenic emissions varying (purple). Included in **b** are tracers of stratospheric ozone ($O_3$Strat, blue) and East Asian pollution (EACOt; orange, right axis). Correlations ($r^2$) in **a** are between observed March–April ozone and the previous November–December–January Niño 3.4, and in **b**–**d** are between observations and simulations. The linear trends in **c** include 95% confidence intervals and *P* values for a two-tailed *t*-test.

Shifts in atmospheric circulation play a key role in the observed ozone increase in autumn and the absence of any change in spring by modulating the Asian pollution reaching MLO. This conclusion is supported both by the COt tracers, which reveal a major influence of circulation-driven changes on the Asian pollution signal in ozone measured at MLO during both spring and autumn, and by the simulation with constant precursor emissions, which simulates an ozone decrease in March and April and captures the observed ozone increase in September and October (Fig. 1b). The simulation in which both emissions and meteorology vary reproduces the small overall observed change in springtime ozone (Fig. 1c), due to an offset of the circulation-driven decrease by rising Asian emissions.

## Drivers of interannual variability in spring

ENSO events are a dominant mode of global climate variability on interannual timescales, and we focus here on the transport

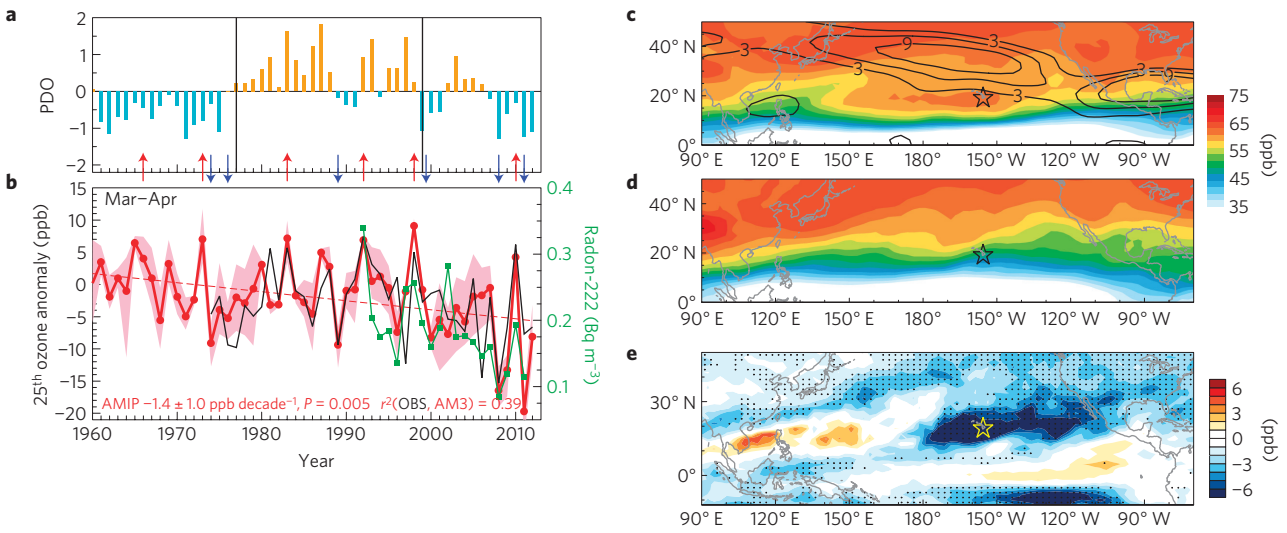


**Figure 4 | Decadal variability and trends for March–April during 1960–2012. a**, The PDO index (see Methods). Indicated are the 1976–1977 and 1998–1999 climate shifts (vertical lines) and strong El Niño (red arrows) and La Niña (blue arrows) events. **b**, Anomalies of 25th percentile of daily ozone relative to 1980–1994 at MLO. Pink shaded regions represent the range of ensemble members. The green line (right axis) indicates observed radon-222. **c**,**d**, Simulated mean ozone at 675 hPa for the El Niño (**c**) and La Niña (**d**) composites. Contours (labelled every 3 m s$^{-1}$) in **c** indicate 250 hPa wind speed anomalies for El Niño relative to normal conditions. **e**, Changes in 25th percentile ozone at 675 hPa for ENSO-neutral springs (2000–2012 minus 1960–1975). Stippling denotes areas where the change is statistically significant ($P < 0.05$).

mechanisms through which ENSO events can influence the variability in springtime ozone distributions at MLO (Fig. 3). The 40 years of MLO observations include four major warm El Niño events and five cold La Niña events (Fig. 3a). Springtime ozone at MLO is observed to increase following El Niño conditions and decrease following La Niña conditions (Fig. 3b), correlating with the Niño 3.4 index from the previous winter ($r^2 = 0.32$). The AM3 simulation with fixed precursor emissions captures ozone interannual variability measured at MLO ($r^2 = 0.53$, Fig. 3b). Observed ozone interannual variability correlates strongly with variations in Asian pollution transport as inferred by the East Asian COt ($r^2 = 0.45$). Changes in stratospheric ozone at MLO also contribute to observed ozone variability ($r^2 = 0.18$), but to a lesser extent than the Asian influence. Despite large El Niño enhancements to wildfire activity in equatorial Asia[31,32], our model sensitivity experiments indicate that wildfire emissions are not the main driver of ENSO-related ozone variability at MLO (Fig. 3d).

The AMIP simulations forced with observed SSTs also capture the ozone variability measured at MLO, further supporting a key role for tropical ocean forcing during ENSO in modulating interannual variability of subtropical free tropospheric ozone in spring (Fig. 4a,b and Supplementary Fig. 3). During an El Niño event, the subtropical jet strengthens across the western Pacific and extends well past the International Date Line (Fig. 4c). This El Niño teleconnection leads to a stronger channelling of mid-latitude air towards Hawaii. Simulated ozone at 675 hPa (~3.5 km) between 10° N and 20° N from 140° E to 140° W increases during El Niño, consistent with increases in equatorward mass flux below 600 hPa over the same region[33]. The La Niña phase manifests in the opposite way (Fig. 4d).

Observations and model simulations consistently indicate that the ENSO-driven change in springtime ozone at MLO involves a shift in the mean as well as a change in the standard deviation ($\sigma$) of daily ozone (Fig. 5a,b). Weaker day-to-day variability occurs during El Niño ($\sigma = 9.6$ ppb), with a strong reduction in the frequency of low-ozone events, compared with La Niña conditions ($\sigma = 12.6$ ppb). This finding is consistent with an equatorward shift of the subtropical jet during El Niño (Fig. 4c), which reduces the influence of ozone-poor tropical air at MLO.

## Drivers of decadal variability and trends in spring

We next use the AMIP simulations over 1960–2012 to explore the decadal signature of ENSO variability in ozone at MLO. The PDO has been described as a long-lived El Niño-like pattern of Pacific climate variability on multi-decadal timescales[22,23]. Figure 4a shows a time series of the PDO index for 1960–2012. In 1976–1977, the PDO changed to the positive phase, tending towards more prolonged and stronger El Niño events[7,34]. There is observational evidence that the PDO shifted back to the negative phase in 1998–1999, with strong La Niña events occurring more frequently since then[34–36]. These decadal shifts in Pacific climate have widespread impacts, including on fisheries[34], mid-latitude droughts[36,37], and the recent global-warming hiatus[38,39]. The impact on atmospheric composition, however, has not been examined.

Here we suggest that the Pacific climate shifts have affected springtime ozone variability at MLO on decadal timescales (Fig. 4b). The shift from a warm (1980–1998) to a cold (1999–2012) PDO regime manifests as a decrease in ozone-rich Eurasian airflow reaching MLO. Supporting this conclusion, observations of radon-222 (indicative of continental influence) at MLO decrease from the 1990s to the 2000s, consistent with the ozone decreases simulated by AM3 with constant precursor emissions (Fig. 4b). Observed ozone shows a larger standard deviation in daily ozone during 2000–2012 versus 1980–1998 as a result of more frequent La Nina events (Fig. 5c), with no significant change in the mean owing to the offsetting effects of tripled Asian emissions[11]. The reduction in Eurasian airflow in spring has also been suggested as contributing to the observed decline in the amplitude of the $CO_2$ seasonal cycle at MLO during 1990–2004 (ref. 40).

In addition to the ENSO/PDO related variability, any widening of the tropical belt since the 1960s (refs 24–26) would increase the influence of ozone-poor tropical air at MLO, which is located in the vicinity of the subsiding branch of the Hadley circulation in spring (Fig. 2a). This longer-term tendency towards greater tropical influence further contributes to the ozone decrease at MLO driven by the La-Niña-like cooling in the eastern equatorial Pacific over the past decade[38,39]. The AMIP ensemble simulations (with constant emissions of ozone precursors) give statistically significant

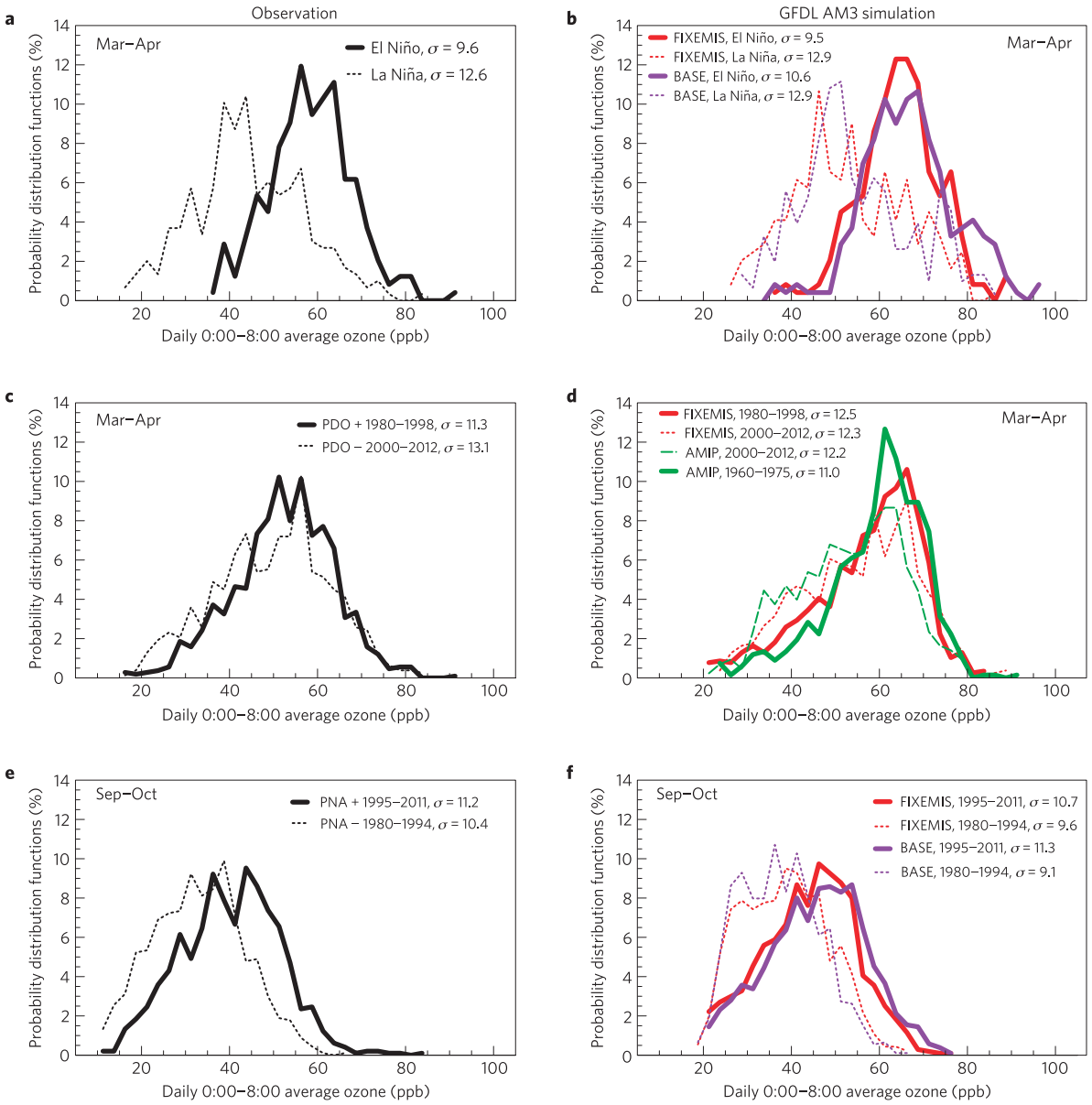


**Figure 5 | Observed (left) and simulated (right) changes in daily ozone distribution at MLO. a**,**b**, For March–April during El Niño versus La Niña. **c**,**d**, For March–April during 1980–1998 versus 2000–2012 corresponding with the PDO shift. The green lines in **d** denote the influence of the tropical expansion for ENSO-neutral years. **e**,**f**, For September–October during 1980–1994 versus 1995–2011 corresponding with the PNA shift. The standard deviation ($\sigma$) is shown, as are model simulations with time-varying (purple) and constant (red and green) emissions. Night time 0:00–8:00 average data are used to represent free tropospheric down-slope conditions observed at the MLO altitude.

($P < 0.001$) decreases of $1.3 \pm 0.7$ ppb per decade in median ozone (Supplementary Fig. 3) and $1.4 \pm 1.0$ ppb per decade in the 25th percentile over the period 1960–2012 (Fig. 4b).

Excluding the interannual variability driven by moderate to strong ENSO events, the model simulates a higher frequency of low-ozone events at MLO in spring during 2000–2012 versus 1960–1975 due to a larger influence from ozone-poor tropical air (Fig. 5d). The largest ozone decrease from the 1960s to the 2000s occurs over the eastern Pacific subtropical region (Fig. 4e), where a statistically significant increase in tropopause heights during 1979–2005, interpreted as evidence for a widening tropical belt, was found[24,41]. However, different diagnostic methods indicate weaker or insignificant widening trends in the tropical belt[27]. It remains an open question whether the long-term spring ozone decrease over the Pacific subtropical region during 1960–2012 documented here implies tropical expansion.

## Drivers of interannual to decadal variability in autumn

Observed ozone concentrations at MLO in September and October show an abrupt increase in the mid-1990s, with a statistically significant ($P < 0.001$) trend of $3.5 \pm 1.4$ ppb per decade over the period 1980–2012 (Fig. 3c). With both meteorology and emissions varying, the GFDL AM3 model simulates an ozone increase of $4.2 \pm 1.6$ ppb per decade ($P < 0.001$) and captures 77% of the observed interannual variability. With ozone precursor emissions held constant, AM3 gives a statistically significant increase of $2.3 \pm 1.6$ ppb per decade and captures the abrupt change near 1995 ($r^2 = 0.66$), implying a meteorological shift. This shift is also captured by the AMIP simulations without nudging (Supplementary Fig. 4). Both observations and model indicate that the dominant change in ozone during autumn from 1980–1994 to 1995–2011 involves an increase in the high tail (above 50 ppb) of the daily distribution (Fig. 5e,f).

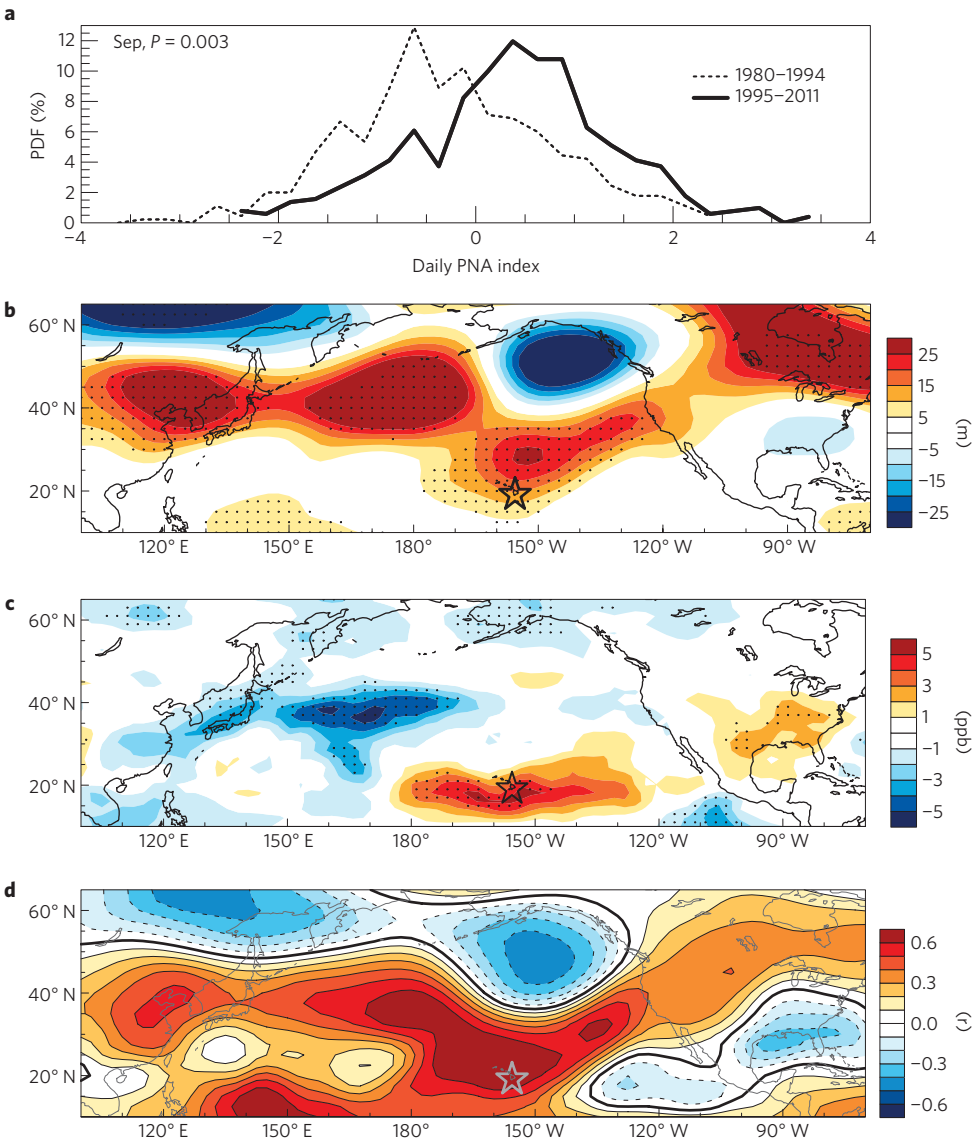


**Figure 6 | Stronger transport of Asian ozone pollution to MLO in September tied to a shift in the PNA pattern in the mid-1990s. a**, Probability distribution functions (PDF) for the daily PNA index (see Methods). **b**,**c**, Changes between two period means (1995–2011 minus 1980–1994), in NCEP/NCAR 500 hPa geopotential heights and in 675 hPa ozone simulated with constant precursor emissions (FIXEMIS), respectively. Stippling denotes areas where the change is statistically significant ($P < 0.05$). **d**, Temporal correlations of September mean MLO ozone with NCEP/NCAR 500 hPa geopotential heights in the domain over 1980 to 2011.

We find that the autumn ozone increase aligns with a period of enhanced ridges near Hawaii since the mid-1990s, tied specifically to a statistically significant ($P = 0.003$) shift in the PNA pattern towards the predominantly positive phase in September (Fig. 6a,b). Changes in the PNA pattern for October are statistically insignificant ($P = 0.173$). Observed changes in 500 hPa geopotential heights for September between 1980–1994 and 1995–2011 resemble the positive phase of PNA, with above-average heights in the vicinity of Hawaii and over the intermountain region of North America, and below-average heights located south of the Aleutian Islands and over the southeastern United States[28,29].

Enhanced ridges near Hawaii during the positive PNA, accompanied by a deepening of the Aleutian Low, provide a channel for mid-latitude pollution over the western North Pacific to descend isentropically towards the south. Simulated ozone at 675 hPa increases south of Hawaii and decreases in the upwind Pacific Ocean regions (Fig. 6c). This southward isentropic transport pathway is reflected in strong positive correlations ($r = 0.5$–$0.7$) of mean geopotential heights with ozone observed at MLO during September (Fig. 6d). Transport of East Asian pollution events to Hawaii in autumn occurred more frequently during 1995–2011 associated with the increasing frequency of the wave-like feature of the positive PNA pattern. The enhancement in transport events is consistent with the observed increases in the high tail (above 50 ppb) of the daily ozone distribution (Fig. 5e).

Nitrogen oxides ($NO_x$) released from PAN, a reservoir species that decomposes when the air warms[42,43], probably add to the ozone increase at MLO during autumn as mid-latitude pollution descends southward to Hawaii. The additional effects of chemistry on ozone during transport are consistent with the larger simulated ozone response to changing meteorology than for the idealized CO tracers. The overall warming of global temperature during this period is unlikely to be the main driver of the abrupt ozone increase at MLO during autumn because warmer temperatures in remote regions enhance ozone destruction and also decrease long-range transport of PAN.

## Signatures of climate variability in ozone measurements

Through a comprehensive analysis of daily to decadal variability in sources of ozone during the past half-century, we have identified the underlying mechanisms controlling the spring versus autumn ozone trends in Hawaiian records previously reported[17]. We identify a key role for decadal climate shifts in modulating the response of tropospheric ozone to a growth in Asian precursor emissions as measured at remote locations. The La-Niña-like decadal cooling in the eastern equatorial Pacific in the 2000s (possibly combined with a widening tropical belt) decreases ozone-rich Eurasian airflow towards the subtropical North Pacific region in spring, offsetting ozone increases in Hawaii that otherwise would have occurred owing to rising Asian emissions. During Autumn, a shift in the PNA pattern towards more frequent positive modes since the mid-1990s has caused Asian ozone pollution reaching Hawaii to rise suddenly.

Our analysis reveals signatures of interannual to decadal climate variability in long-term tropospheric ozone measurements. Changes in tropospheric ozone observed at other Northern Hemisphere remote sites[9,14–16] may be similarly influenced by decadal shifts in atmospheric circulation patterns, although the specific circulation regimes and sources of ozone influencing each location will need to be identified. Decadal climate variability has the potential to offset or augment the effects of changing emissions, and thus must be considered when attributing observed ozone changes to human-induced trends in precursor emissions.

## Methods

**Observations.** The surface ozone measurements at MLO have been made with ultraviolet absorption analysers from 1976 to present. In the initial period of observations from 1973 to 1975, an electrochemical instrument was used. Several years of overlapping observations have been employed in transition from one instrument to another[8]. Through the entire measurement record, the observations have been calibrated to the US National Institute of Standards and Technology (NIST) ozone reference through comparison to a NOAA/ESRL Global Monitoring Division network standard, which in turn has been periodically compared to the NIST standard. The instrument accuracy is about ±2%. No instrumental drift has been reported in the MLO ozone record. The radon-222 data at MLO were compiled from observations obtained from two measurement programmes and three different instrument configurations. The measurements were adjusted to the same NIST standard, according to ref. 44. We use measurements averaged over 0:00–8:00 local time when observed conditions at the 3.4 km altitude of MLO represent down-slope influence of free tropospheric air.

**Chemistry–climate model experiments.** We conduct a suite of hindcast simulations with the GFDL AM3 chemistry–climate model at ~200 × 200 km$^2$ horizontal resolution (Supplementary Table 1), which includes interactive stratosphere–troposphere chemistry and aerosols[18]. Three AM3 simulations (BASE, FIXEMIS, IAVFIRE) were nudged to National Centers for Atmospheric Prediction and National Center for Atmospheric Research (NCEP/NCAR) reanalysis winds from 1980 to 2012, using a pressure-dependent nudging technique as described previously[19,20]. We avoid using the reanalysis data for before 1979 owing to the discontinuity of satellite data assimilated into the reanalysis. The AMIP simulations (3 ensemble members with different initial conditions) are driven by the observed evolution of SSTs, sea ice, and atmospheric radiative forcing agents from 1960 to 2012. Human-induced emissions of ozone precursors and the methane lower boundary condition for chemistry are held constant in FIXEMIS, IAVFIRE and AMIP simulations. A detailed description of emission data and model initialization is provided in Supplementary Information.

We implement a set of regional CO-like tracers[45] to investigate the role of circulation-driven changes in hemispheric pollution transport. The CO tracers have 50-day exponential lifetime and surface emissions constant in time from each of four northern mid-latitude source regions (Supplementary Fig. 2). To quantify stratospheric influence, we define a stratospheric ozone tracer relative to a dynamically varying tropopause and subject it to chemical and depositional loss in the same manner as ozone in the troposphere, as described previously[20].

**Climate indices.** The Niño 3.4 index is based on the running 3-month SST anomaly over 5° N–5° S latitudes and 120°–170° W longitudes obtained from the NOAA Climate Prediction Center. Events with |Niño3.4| ≥ 1.0 for at least five consecutive months are categorized as moderate to strong ENSO episodes (excluding the 1987/1988 El Niño when the Niño 3.4 index anomalously peaked in the late summer, Fig. 3a). Other years are classified as ENSO-neutral years.

The PDO index is defined as the leading principal component of North Pacific monthly SST variability (http://jisao.washington.edu/pdo/PDO.latest)[22]. The PNA index is downloaded from the NOAA Climate Prediction Center: it is derived from the rotated principal component analysis of 500 hPa geopotential height anomalies[28].

Received 5 July 2013; accepted 12 December 2013; published online 26 January 2014

## References


1. Stevenson, D. S. *et al.* Multimodel ensemble simulations of present-day and near-future tropospheric ozone. *J. Geophys. Res.* **111,** D08301 (2006).
2. Jacob, D. J., Logan, J. A. & Murti, P. P. Effect of rising Asian emissions on surface ozone in the United States. *Geophys. Res. Lett.* **26,** 2175–2178 (1999).
3. Hemispheric Transport of Air Pollution 2010—Part A Ozone and Particulate Matter (United Nations Economic Commission for Europe, Geneva, 2010).
4. Langford, A. O., O'Leary, T. J., Masters, C. D., Aikin, K. C. & Proffitt, M. H. Modulation of middle and upper tropospheric ozone at northern midlatitudes by the El Nino Southern Oscillation. *Geophys. Res. Lett.* **25,** 2667–2670 (1998).
5. Lelieveld, J. & Dentener, F. J. What controls tropospheric ozone? *J. Geophys. Res.* **105,** 3531–3551 (2000).
6. Koumoutsaris, S., Bey, I., Generoso, S. & Thouret, V. Influence of El Nino-Southern Oscillation on the interannual variability of tropospheric ozone in the northern midlatitudes. *J. Geophys. Res.* **113,** D19301 (2008).
7. *IPCC Climate Change 2007: The Physical Science Basis* (Cambridge Univ. Press, 2007).
8. Oltmans, S. J. *et al.* Tropospheric ozone during Mauna Loa observatory photochemistry experiment 2 compared to long-term measurements from surface and ozonesonde observations. *J. Geophys. Res.* **101,** 14569–14580 (1996).
9. Oltmans, S. J. *et al.* Recent tropospheric ozone changes—A pattern dominated by slow or no growth. *Atmos. Environ.* **67,** 331–351 (2013).
10. Richter, A., Burrows, J. P., Nuss, H., Granier, C. & Niemeier, U. Increase in tropospheric nitrogen dioxide over China observed from space. *Nature* **437,** 129–132 (2005).
11. Granier, C. *et al.* Evolution of anthropogenic and biomass burning emissions of air pollutants at global and regional scales during the 1980–2010 period. *Climatic Change* **109,** 163–190 (2011).
12. Ohara, T. *et al.* An Asian emission inventory of anthropogenic emission sources for the period 1980–2020. *Atmos. Chem. Phys.* **7,** 4419–4444 (2007).
13. Warneke, C. *et al.* Multiyear trends in volatile organic compounds in Los Angeles, California: Five decades of decreasing emissions. *J. Geophys. Res.* **117,** D00V17 (2012).
14. Cooper, O. R. *et al.* Increasing springtime ozone mixing ratios in the free troposphere over western North America. *Nature* **463,** 344–348 (2010).
15. Parrish, D. D. *et al.* Long-term changes in lower tropospheric baseline ozone concentrations at northern mid-latitudes. *Atmos. Chem. Phys.* **12,** 11485–11504 (2012).
16. Logan, J. A. *et al.* Changes in ozone over Europe: Analysis of ozone measurements from sondes, regular aircraft (MOZAIC) and alpine surface sites. *J. Geophys. Res.* **117,** D09301 (2012).
17. Oltmans, S. J. *et al.* Long-term changes in tropospheric ozone. *Atmos. Environ.* **40,** 3156–3173 (2006).
18. Donner, L. J. *et al.* The Dynamical Core, Physical Parameterizations, and Basic Simulation Characteristics of the Atmospheric Component AM3 of the GFDL Global Coupled Model CM3. *J. Clim.* **24,** 3484–3519 (2011).
19. Lin, M. Y. *et al.* Transport of Asian ozone pollution into surface air over the western United States in spring. *J. Geophys. Res.* **117,** D00V07 (2012).
20. Lin, M. Y. *et al.* Springtime high surface ozone events over the western United States: Quantifying the role of stratospheric intrusions. *J. Geophys. Res.* **117,** D00V22 (2012).
21. Trenberth, K. E. *et al.* Progress during TOGA in understanding and modeling global teleconnections associated with tropical sea surface temperatures. *J. Geophys. Res.* **103,** 14291–14324 (1998).
22. Mantua, N. J., Hare, S. R., Zhang, Y., Wallace, J. M. & Francis, R. C. A Pacific interdecadal climate oscillation with impacts on salmon production. *Bull. Am. Meteorol. Soc.* **78,** 1069–1079 (1997).
23. Knutson, T. R. & Manabe, S. Model assessment of decadal variability and trends in the tropical Pacific Ocean. *J. Clim.* **11,** 2273–2296 (1998).
24. Seidel, D. J., Fu, Q., Randel, W. J. & Reichler, T. J. Widening of the tropical belt in a changing climate. *Nature Geosci.* **1,** 21–24 (2008).
25. Allen, R. J., Sherwood, S. C., Norris, J. R. & Zender, C. S. Recent Northern Hemisphere tropical expansion primarily driven by black carbon and tropospheric ozone. *Nature* **485,** 350–354 (2012).
26. Lu, J., Deser, C. & Reichler, T. Cause of the widening of the tropical belt since 1958. *Geophys. Res. Lett.* **36,** L03803 (2009).
27. Davis, S. M. & Rosenlof, K. H. A multidiagnostic intercomparison of tropical-width time series using reanalyses and satellite observations. *J. Clim.* **25,** 1061–1078 (2012).

28. Barnston, A. G. & Livezey, R. E. Classification, seasonality and persistence OF low-frequency atmospheric circulation patterns. *Mon. Weath. Rev.* **115,** 1083–1126 (1987).
29. Quadrelli, R. & Wallace, J. M. A simplified linear framework for interpreting patterns of Northern Hemisphere wintertime climate variability. *J. Clim.* **17,** 3728–3744 (2004).
30. Cooper, O. R. *et al.* Direct transport of midlatitude stratospheric ozone into the lower troposphere and marine boundary layer of the tropical Pacific Ocean. *J. Geophys. Res.* **110,** D23310 (2005).
31. Van der Werf, G. R. *et al.* Continental-scale partitioning of fire emissions during the 1997 to 2001 El Nino/La Nina period. *Science* **303,** 73–76 (2004).
32. Duncan, B. N., Martin, R. V., Staudt, A. C., Yevich, R. & Logan, J. A. Interannual and seasonal variability of biomass burning emissions constrained by satellite observations. *J. Geophys. Res.* **108,** 4100 (2003).
33. Waliser, D. E., Shi, Z., Lanzante, J. R. & Oort, A. H. The Hadley circulation: Assessing NCEP/NCAR reanalysis and sparse *in situ* estimates. *Clim. Dyn.* **15,** 719–735 (1999).
34. Chavez, F. P., Ryan, J., Lluch-Cota, S. E. & Niquen, M. From anchovies to sardines and back: Multidecadal change in the Pacific Ocean. *Science* **299,** 217–221 (2003).
35. Overland, J., Rodionov, S., Minobe, S. & Bond, N. North Pacific regime shifts: Definitions, issues and recent transitions. *Prog. Oceanogr.* **77,** 92–102 (2008).
36. Bond, N. A., Overland, J. E., Spillane, M. & Stabeno, P. Recent shifts in the state of the North Pacific. *Geophys. Res. Lett.* **30,** 2183 (2003).
37. Hoerling, M. & Kumar, A. The perfect ocean for drought. *Science* **299,** 691–694 (2003).
38. Meehl, G. A., Hu, A. X., Arblaster, J. M., Fasullo, J. & Trenberth, K. E. Externally forced and internally generated decadal climate variability associated with the Interdecadal Pacific Oscillation. *J. Clim.* **26,** 7298–7310 (2013).
39. Kosaka, Y. & Xie, S-P. Recent global-warming hiatus tied to equatorial Pacific surface cooling. *Nature* **501,** 403–407 (2013).
40. Buermann, W. *et al.* The changing carbon cycle at Mauna Loa Observatory. *Proc. Natl Acad. Sci. USA* **104,** 4249–4254 (2007).
41. Seidel, D. J. & Randel, W. J. Recent widening of the tropical belt: Evidence from tropopause observations. *J. Geophys. Res.* **112,** D20113 (2007).
42. Moxim, W. J., Levy, H. & Kasibhatla, P. S. Simulated global tropospheric PAN: Its transport and impact on NOx. *J. Geophys. Res.* **101,** 12621–12638 (1996).
43. Fischer, E. V., Jaffe, D. A., Reidmiller, D. R. & Jaegle, L. Meteorological controls on observed peroxyacetyl nitrate at Mount Bachelor during the spring of 2008. *J. Geophys. Res.* **115,** D03302 (2010).
44. Chambers, S. D., Zahorowski, W., Williams, A. G., Crawford, J. & Griffiths, A. D. Identifying tropospheric baseline air masses at Mauna Loa Observatory between 2004 and 2010 using radon-222 and back trajectories. *J. Geophys. Res.* **118,** 992–1004 (2013).
45. Fang, Y. *et al.* The impacts of changing transport and precipitation on pollutant distributions in a future climate. *J. Geophys. Res.* **116,** D18303 (2011).


## Acknowledgements

This work was supported by NOAA's Cooperative Institute for Climate Science at Princeton University. We thank I. Held, H. Levy II and P. Ginoux for insightful discussion and comments on the manuscript. The dedication of the MLO staff in maintaining the 40-year observational record is an exceptional accomplishment. The radon-222 data were provided by the US Department of Energy, Environmental Monitoring Laboratory (1991–1996) and the Australian Nuclear Science and Technology Organization (ANSTO) (1997–2011). Discussion with S. Chambers of ANSTO provided information for harmonizing the Radon data sets.

## Author contributions

M.Y.L. conceived the study, performed model experiments, analysed the data, and wrote the manuscript with input from all coauthors. L.W.H., A.M.F. and S.F. assisted M.Y.L. with model experiments and discussed the results. S.J.O. provided the ozone and radon measurements and guided interpretation of the data sets. All authors edited and commented on the manuscript.

## Additional information

Supplementary information is available in the online version of the paper. Reprints and permissions information is available online at www.nature.com/reprints. Correspondence and requests for materials should be addressed to M.Y.L.

## Competing financial interests

The authors declare no competing financial interests.